Electrochimica Acta 308 (2019) 307–316

Contents lists available at ScienceDirect

Electrochimica Acta

journal homepage: www.elsevier.com/locate/electacta

Assembly and electrochemistry of carbon nanomaterials at the liquid-liquid interface

Andrew N.J. Rodgers, Aminu K. Rabiu [1], Peter S. Toth [2], Ralph W. Adams, Robert A.W. Dryfe*

School of Chemistry, University of Manchester, Oxford Road, Manchester, M13 9PL, United Kingdom

ARTICLE INFO

Article history:
Received 8 January 2019
Received in revised form
4 April 2019
Accepted 6 April 2019
Available online 8 April 2019

Keywords:
Bipolar electrochemistry
Liquid-liquid electrochemistry
Nanoparticle
Graphene
Soft interfaces

ABSTRACT

The interfacial adsorption of single-walled carbon nanotubes and few-layer graphene flakes, prepared by solution phase exfoliation, is compared. Strong adsorption of carbon nanotubes was observed at the water/1,2-dichloroethane interface, while a weaker adsorption of the graphene dispersion was seen. Addition of electrolyte to the organic phase was found to have a strong effect on the adsorption of graphene. A simple surface energy model does not fully explain these observations, rather residual charges and their distribution appears to be the key factor behind this difference in adsorptive behaviour. Carbon nanomaterials adsorbed at the liquid-liquid interface can function as bipolar electrodes: a preliminary investigation of the oxidation of the 1,2-dichlorobenzene by metal-modified graphene particles is performed.

1. Introduction

Bipolar electrochemistry uses an external potential difference to polarise an object suspended in an electrolyte. If a sufficiently large electric field is imposed, the polarisation of the object can drive opposing redox reactions on either "face" of the object [1,2]: this approach has been widely exploited as a route to in situ "Janus" functionalization [3]. One drawback of this bipolar functionalization, however, is that increasingly large potential differences must be applied to impose a potential difference capable of driving opposing reactions across an object as the characteristic size of the latter shrinks. This restriction makes it difficult, in practice, to perform Janus functionalization of materials with bipolar electrochemistry where the object's characteristic size approaches the nanometre scale.

Electrochemistry at the interface between two immiscible electrolyte solutions (ITIES) also represents a method to perform "contactless" electrochemistry [4,5]. In a conventional bipolar cell, beyond the controlling electrodes, the potential drop occurs uniformly thorough the bulk of the solution, so only a small proportion of this potential drop will fall across the solution in the vicinity of the suspended object. In contrast for an ITIES cell, most of the potential drop applied to the solution will occur within the "back to back" electrical double layers formed on either side of the liquid-liquid interface [6,7]. Particles, including nanoparticles, can be adsorbed or formed by chemical reaction (e.g. metal deposition) at the liquid-liquid interface [8,9]. Thus, in the case of the ITIES, these adsorbed particles can be exposed to an external electric field, which may in turn affect their adsorption equilibrium [10]. Metal particles can be deposited through electrochemical deposition at this interface [11], and other conducting particles can function as electrocatalysts [12,13].

Conducting particles deposited in this way at the ITIES function as bipolar electrodes with a (catalytic) reduction such as hydrogen evolution occurring on the face in contact with the aqueous phase, and a concomitant oxidation of an electron donor taking place at the organic side of the particle [14]. In fact, two "catalytic" functions of the adsorbed particle may be discerned: it may function as an electrocatalyst in the traditional sense for a multi-step electron transfer, but it may also serve to speed up the overall redox process by acting as an interfacial reservoir of charge, lifting the normal restriction at the ITIES that electron transfer requires the two participants to diffuse to the same region of the interface at the same

* Corresponding author.
E-mail address: robert.dryfe@manchester.ac.uk (R.A.W. Dryfe).
[1] Present address: Pure & Applied Chemistry, Kebbi State University of Science and Technology, Aliero, Nigeria.
[2] Present address: Department of Physical Chemistry & Material Science, University of Szeged, Rerrich Sq 1, H-6720 Szeged, Hungary.

https://doi.org/10.1016/j.electacta.2019.04.035
0013-4686/

time [15]. The process of Fermi level equilibration by such particles, in an electrocatalytic context, has been considered [16]. Simplified equivalent circuit diagrams for the four cases of a standard electrochemical cell, a single-phase cell with an object functioning as a bipolar electrode, an ITIES cell and an ITIES cell with an adsorbed solid functioning as a bipolar electrode are shown in Fig. 1. Note the terminal electrodes have been omitted in each case, for simplicity.

There has been interest in the use of carbon nanomaterials, derived from 1D (carbon nanotubes) and 2D (graphene) materials, as electrocatalysts [17]. There has been considerable debate about the intrinsic electrochemical/electrocatalytic properties of these materials: doped materials, either using heteroatoms incorporated at the time of growth or noble metal nanoparticles deposited on the substrates subsequently, have received much attention. Adsorption of carbon nanotubes and graphene sheets at the liquid-liquid interface has been widely reported [18,19], often as a means to prepare conducting films of these materials. In the specific context of the ITIES, our laboratory has reported that CVD graphene can be adsorbed at this interface and functionalised symmetrically, or asymmetrically, with metal nanoparticles [20–22]. The electrocatalytic properties of such materials have been studied [15,22]. Similar approaches can be used with carbon nanotubes, with the liquid-liquid method used to prepare composites of carbon nanotubes and conducting polymers [23]. Although we have previously reported the effect of addition of electrolyte on organic phase dispersions of graphene [24], in this manuscript we describe the distinct differences in interfacial adsorption seen for graphene and carbon nanotube dispersions. As noted above, we have exploited the adsorption of both classes of carbon nanomaterial at the ITIES for their use as bipolar electrodes in processes as diverse as oxygen reduction [15], with un-functionalised few layer graphene, metal deposition reactions on CVD graphene [20,21], and formation of CNT-polymer composites [23]. We have noted differences in the adsorption of these materials, however, which show a notable sensitivity to the presence of electrolyte in the organic phase electrolyte. As this topic has been little explored in the literature, and affects bipolar electrochemistry at the ITIES in particular, we report a comparative study of the adsorption behaviour in this work. We also describe the use of metal-functionalised graphene particles as bipolar electro-catalysts for partial oxidation of organic molecules.

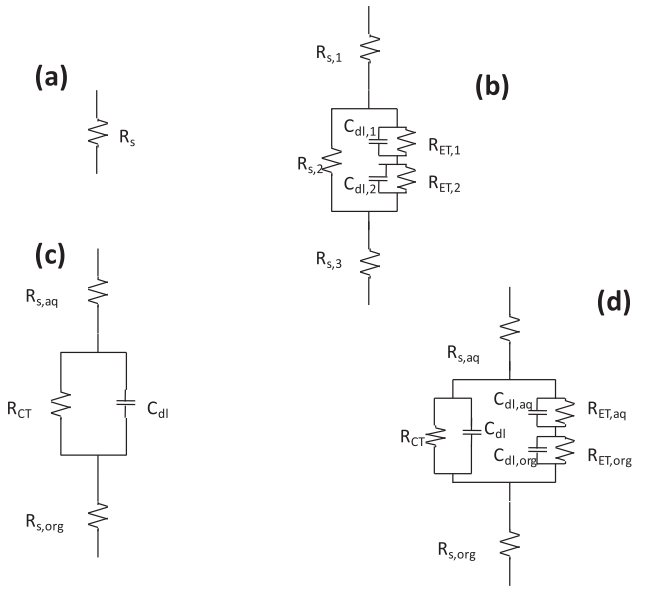

Fig. 1. Simplified equivalent circuit diagrams of (a) an electrochemical cell, (b) a single-phase cell with an object functioning as a bipolar electrode, (c) an ITIES cell and (d) an ITIES cell with an adsorbed solid functioning as a bipolar electrode. R_s represents solution resistance, with aq and org suffixes representing the aqueous and organic phases, respectively, in the ITIES cases. $R_{CT/ET}$ denotes the resistances to charge transfer across the ITIES or the faces of the bipolar electrode. C_{dl} represents the double-layer capacitance of the bipolar electrodes and ITIES.

2. Experimental

2.1. Chemicals and materials

All chemicals were used as received. SWCNTs (arc discharge, >95% carbon), 1, 2-dichloroethane (DCE, ≥99.8%), 1,2-dichlorobenzene (DCB, ≥99%), hexane (99%), 1-hexanol (99%), lithium chloride (LiCl, ≥99%), potassium tetrakis (4-chlorophenyl) borate (KTPBCl, ≥98%), bis(triphenylphosporanylidene)ammonium chloride (BTPPACl, 97%) %), ammonium tetrachloropalladate (II) ($(NH_4)_2PdCl_4$, 99.995%) and ammonium tetrachloroplatinate (II) ($(NH_4)_2PtCl_4$, 99%) were purchased from Sigma-Aldrich, UK. Ammonium persulfate (98%) was supplied by Lancaster Synthesis Ltd. Natural graphite flakes (2369) were supplied by Graphexel Ltd., UK. The CVD grown monolayer graphene was provided by BGT Materials Ltd. (Manchester, UK), characterisation of this material has been reported by us in previous works [20,21]. Bis(-triphenylphosporanylidene)ammonium tetrakis (4-chlorophenyl) borate (BTPPATPCl) was synthesised, by metathesis of BTPPACl and KTPBCl, as described previously [25]. A slight deviation from this procedure was applied, with a solvent mixture of 2:1:1 acetone:ethanol:water used for the metathesis reaction and a mixture of 1:1 acetone:ethanol used for the recrystallisation step. Ultra-pure water (18.2 MΩ cm resistivity) was obtained from a "Milli Q direct" water purification system, Merck Millipore.

2.2. Graphene and SWCNT dispersion

Dispersions of graphene and SWCNTs were prepared by bath sonication (Elmasonic P70H, Elma GmbH & Co. KG, at 37 KHz) in organic solvent (DCE or DCB). Graphene dispersions were sonicated for 2 h (70% power) and SWCNT dispersions for 12 h (30% power). The starting concentrations were 100 μg ml^{-1} and 9 μg ml^{-1}, for graphene and SWCNT dispersions, respectively. Larger particles and aggregates were removed from the graphene dispersions using the previously reported procedure [15,24], adapted from the work of Coleman *et. al.* [26], of standing for 24 h followed by centrifugation (587 rpm, 45 min) of the supernatant, with the resulting supernatant taken as the final dispersion. SWCNT dispersions were simply centrifuged at 15000 rpm for 60 min and the supernatant taken as the final dispersion [27]. Note, despite the differing initial concentrations of the two materials, the supernatant (formed from the stable dispersion) was used for subsequent liquid-liquid assembly.

Characterisation of the dispersed materials was performed using scanning electron microscopy (SEM, FEI XL30 Environmental Scanning Electron Microscope-Field Emission Gun, FEI Company, USA), atomic force microscopy (AFM, Multimode® 8 Atomic Force Microscope, Bruker, USA) and Raman spectroscopy (532 nm excitation laser, inVia Raman Spectrometer, Renishaw, UK). For these measurements, the graphene and SWCNT dispersions were diluted with pure DCE solvent, at a ratio of ca. 1:2 dispersion:DCE, and drop cast onto a hot Si/SiO_2 wafer.

2.3. Liquid|Liquid assembly of dispersions

For assembly at the liquid|liquid interface, an equal volume of aqueous phase was added on top of the organic dispersion of graphene/SWCNTs and mild sonication (30% power, 37 kHz) was

applied to the cell for 1–15 min [15,23,27,28]. Cells were left to stand overnight, to allow time for attachment and assembly of the dispersed materials at the liquid|liquid interface. All assembly experiments were performed in screw-top vials.

2.4. Contact angle and interfacial tension measurements

Contact angle and interfacial tension measurements were performed using an Attension Theta optical tensiometer (Biolin scientific, Finland). For three-phase contact angle measurements, the organic phase was used as the sessile drop and the aqueous phase as the surrounding phase, due to the greater density of the organic phase. In order to report contact angles with respect to the aqueous phase, in line with convention, all values recorded in this setup were subtracted from 180°. HOPG was used as a comparable substitute material for graphene contact angle measurements and the surface was freshly cleaved prior to each measurement. For SWCNT contact angle measurements, assembled SWCNT films were collected from the water|DCE interface on a Si/SiO_2 wafer. A fresh SWCNT film was used for each measurement.

2.5. Modification of CVD graphene and electrochemical measurements

Macroscopic (several mm diameter) flakes of monolayer CVD graphene were functionalised either onthe top-side only or asymmetrically with transition metal nanoparticles, using an approach we have described previously [21,22]. Briefly, the CVD graphene was decorated by either Pt or Pd nanoparticles (NPs) using a redox reaction between the copper foil substrate of the graphene layer and tetrachlorometal salts (either $(NH_4)_2PdCl_4$, $(NH_4)_2PtCl_4$) forming the corresponding metallic nanoparticles. Then, the copper foil under the CVD GR was removed by etching with ammonium persulfate. In the case on Pd/GR composite, the copper foil was only partially removed resulting in a Pd/GR/Cu asymmetrically decorated graphene layer [22]. The as-prepared Pt/GR, Pd/GR, or Pd/GR/Cu composite films adsorb at the upper (air) surface of the aqueous etch bath and were transferred from there using a Si/SiO_2 wafer and rinsed three times with pure water for cleaning, and then transferred to the top of 6 M LiCl aqueous solution in the L/L glass cell. Subsequently the organic phase was added on top of the aqueous phase. Note the organic phase contained hexane (see Table 2), which along with the high aqueous phase electrolyte concentration, inverted the phases so that the aqueous phase became the lower phase. When employed as bipolar electrodes in the oxidation experiments, the Pt and Pd were oriented to be adjacent to the organic phase, while the Cu particles faced the aqueous phase. For the electrochemical studies at the modified ITIES, cyclic voltammetric and chronoamperometric experiments were performed using a four-electrode configuration with an Autolab PGSTAT100 potentiostat (Metrohm-Autolab). Homemade Ag/AgCl reference electrodes (RE) were directly immersed in the chloride-containing aqueous phase, an aqueous solution of 0.1 mM LiCl and 1 mM BTPPACl was brought in contact with the organic solution formed a liquid junction for the organic reference electrode. The aqueous counter electrode (CEw) was glass coated to avoid contact of the Pt with the organic (upper) phase (all metals were obtained from Advent Research Materials).

2.6. NMR spectroscopy of interfacial oxidation

NMR measurements were performed on a Bruker 500 AVIII HD 500 spectrometer with 5 mm prodigy BBO probe. As well as conventional ^1H acquisition, NMR experiments were run using solvent-signal pre-saturation or selective excitation to remove the large protio-solvent hexane signals, overcoming issues relating to dynamic range and increasing the sensitivity to hexanol (also present in the organic phase) signals. Each of the samples was transferred directly from the electrochemical cell to a 5 mm diameter NMR tube. The spectra were gradient-shimmed using the strongest signal from the solvent and run in the absence of a deuterium lock.

3. Results and discussion

3.1. General assembly at the Liquid|Liquid interface

The assembly of both few-layer graphene and SWCNTs at the liquid|liquid interface was studied here. Water|DCE was the primary system used, though some preliminary work also used the water|DCB interface. These two systems were chosen due to their common employment as solvents in electrochemical studies at the interface between two immiscible electrolyte solutions (ITIES) [4,5], which provide an interesting platform for electrochemical study of such graphitic nano-material assemblies [12,14,15,20,23,27,28].

Dispersions of the carbon nano-materials were first prepared in the organic phase, to which the aqueous phase was then added, thus forming the liquid|liquid interface. The entire system was gently sonicated, to bring about interfacial attachment and assembly of the graphitic materials. The assembled materials were characterised *in-situ*, using optical microscopy.

Attachment and assembly of the graphitic materials at the liquid|liquid interface was probed in the presence and absence of electrolyte in each of the liquid phases. In order to rationalise the observed effects of electrolyte, the interfacial tension and contact angle (formed with the interfacial material) was also studied as a function of electrolyte concentration in each phase.

3.2. Graphene assembly

Natural graphite flakes were exfoliated in DCE at a starting concentration of 100 $\mu g\,ml^{-1}$, using sonication. The resultant dispersion was centrifuged to remove larger, unexfoliated flakes, leaving behind a dispersion of few-to multi-layer graphene, with an average flake length (longest lateral dimension) of 411 nm. Characterisation of the dispersed flakes with optical microscopy (Fig. S1) and Raman spectroscopy (Fig. S2) is presented in the Supporting Information. The concentration of the graphene dispersion was calculated to be 19 $\mu g\,ml^{-1}$, using UV–Vis absorption spectroscopy, assuming the extinction coefficient of $2305 \pm 24\,ml\,mg^{-1}\,m^{-1}$, as previously determined in our laboratory [27]. After addition of an equal volume of aqueous phase to the dispersion, sonication was used to bring about attachment of the exfoliated graphene at the water|DCE interface.

Fig. 2 shows a 24 h time-lapse, immediately following sonication, in which the gradual attachment of graphene at the water DCE interface is seen. Four different water| DCE interfaces were used, containing different combinations of the electrolytes $LiCl_{(aq)}$ and $BTPPATPBCl_{(DCE)}$: **a**) water |DCE, **b**) 0.1 M $LiCl_{(aq)}$ |DCE, **c**) water | 10 mM $BTPPATPBCl_{(DCE)}$ and **d**) 0.1 M $LiCl_{(aq)}$ |10 mM $BTPPATPBCl_{(DCE)}$. These electrolytes were chosen due to their common use in electrochemical studies at the ITIES. Note that the 10 mM concentration chosen in the case of organic electrolyte is close to the solubility of this electrolyte in DCE. The formation of air bubbles at the liquid interface, as seen in cell d (Fig. 2), is a common side effect of interfacial sonication, although it does not appear to affect the attachment of particles at the liquid interface.

In the absence of organic electrolyte (cells a and b, Fig. 2) graphene was seen to attach to both the water |DCE interface and the interface between the DCE phase and the walls of the glass cell.

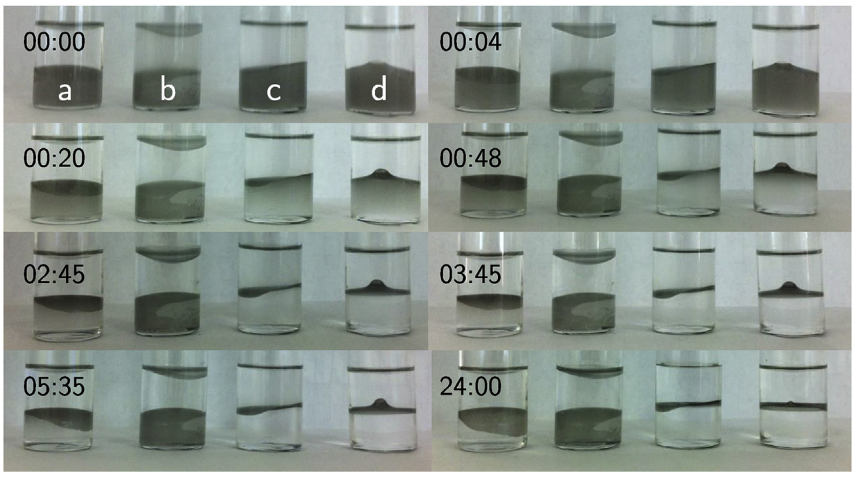

Fig. 2. Photographs showing attachment of a 19 μg ml^{-1} graphene dispersion, initially dispersed in DCE, at the water|DCE interface. The time after sonication of the interface, used to bring about interfacial attachment, is displayed in hours and minutes. Different combinations of electrolyte were present in each cell. **a**) Water DCE, **b**) 0.1 M $LiCl_{(aq)}$|DCE, **c**) Water|10 mM $BTPPATPBCl_{(DCE)}$, **d**) 0.1 M $LiCl_{(aq)}$ 10 mM $BTPPATPBCl_{(DCE)}$.

Attachment at the cell walls was also observed by Woltornist et al.,[15] in a water|heptane system [29], and attributed to the hydrophilic nature of glass leading to the formation of a thin film of water at the cell walls within the organic phase and, thus, a second liquid interface at which the graphene can attach. A three-phase contact angle (θ) of 11.6° (Supporting Information, Fig. S3), measured here for the water |glass| DCE interface, confirmed the hydrophilic nature of the glass cell walls in our configuration.

The addition of electrolyte to the DCE phase (cells c and d, Fig. 2) significantly affected the interfacial attachment behaviour of graphene, with only attachment at the water| DCE interface observed and none at the cell wall| DCE interface. The possibility that addition of organic electrolyte significantly changes the energetics of interaction between water, DCE and glass (thus stopping the thin-layer of water forming along the cell walls within the organic phase) was ruled out by measurement of θ values within ca. 3° of one another for the water |glass |DCE interface in the presence and absence of organic electrolyte (Supporting Information, Figs. S3 and S4). In the water| DCE system (cell a, Fig. 2), the graphene appears to first attach at the water DCE interface, followed by subsequent growth along the cell walls. Based upon this behaviour, we propose that attachment at the liquid interface is favoured most, with attachment at the cell walls following, once the liquid|liquid interface is saturated. Thus, adding electrolyte to the organic phase appears to result in an increase in the saturation limit of the water| DCE interface with respect to graphene. This hypothesis was further strengthened upon repeating the experiment with higher concentration graphene dispersions (100 μg ml^{-1}) in 1,2-dichlorobenzene (DCB), which had not been centrifuged to remove the larger unexfoliated flakes. At this concentration, the cells containing no organic electrolyte could not support all of the graphene at the water| DCB interface, with much of the graphene left in dispersion in the organic phase, while the cells containing organic electrolyte were able to support the majority of graphene at the water |DCB interface.

In-situ optical microscopy (Fig. 3) of the water |DCE interface showed that, in the absence of organic electrolyte, discrete clusters of graphene flakes were present. Conversely, in the presence of organic electrolyte, the interfacial graphene flakes assembled to form a more compact film, as evidenced by the presence of wrinkles in the film at the water|DCE interface. Higher magnification micrographs of these interfacial graphene films are shown in Fig. S5 of the Supporting Information. This improvement in film coherency, initiated simply upon addition of organic electrolyte, is very relevant in the context of using liquid interfacial assembly to prepare graphene films for use as electrodes and in devices such as solar panels, sensors and flexible electronics. In these applications, the quality of the flake-to-flake contacts is a critical factor in maximising the electrical and mechanical properties of the graphene films [19,29,30].

It is also clear that there are a significant number of droplets at the interfaces of the cells containing organic electrolyte (c and d, Fig. 3). These droplets are thought to be formed during sonication of the liquid cells, which leads to a certain amount of emulsification of the water and DCE phases. This is evidenced by the cloudy nature of the various DCE phases in Fig. 3, immediately after sonication. Assembly of graphene flakes around the droplets, in cells c and d (Fig. 3), stabilises them against coalescence. This was evidenced by the observation of various spherical arrays of graphene after collection of assembled films from the interfaces of cells c and d (from Fig. 3, see also Supporting Information, Fig. S6).

Thus far, it has been established that adding electrolyte to the organic phase results in formation of a more coherent film of graphene at the liquid|liquid interface and allows a greater density of graphene to be supported at the interface. It is likely that the latter effect is a result of the former, with more graphene flakes being packed at the liquid|liquid interface due to closer flake-to-flake contacts.

To understand the causes of these effects, we must consider how the organic electrolyte affects both the energetics of interfacial attachment/assembly and the interactions between graphene flakes at the water| DCE interface. The ultimate driving force for both attachment and assembly at a liquid|liquid interface is a reduction in the overall free energy of the system [31,32]. This process can be quantified through the Gibbs energy of adsorption (ΔE), which is the energy required to remove a particle from the interface. In the simplest “surface energy” model of interfacial adsorption, which neglects electrostatic or capillary effects, three main variables affect ΔE: the interfacial tension of the aqueous organic interface ($\gamma_{w|o}$), the particle size and θ of the aqueous| particle| organic interface. θ Is a function of γ for the w o, particle|aqueous (p|w) and particle|organic (p| o) interfaces, as described by Young's equation (1). Equation (2), as derived by Creighton et al. [33], is an approximate form of ΔE for thin platelets

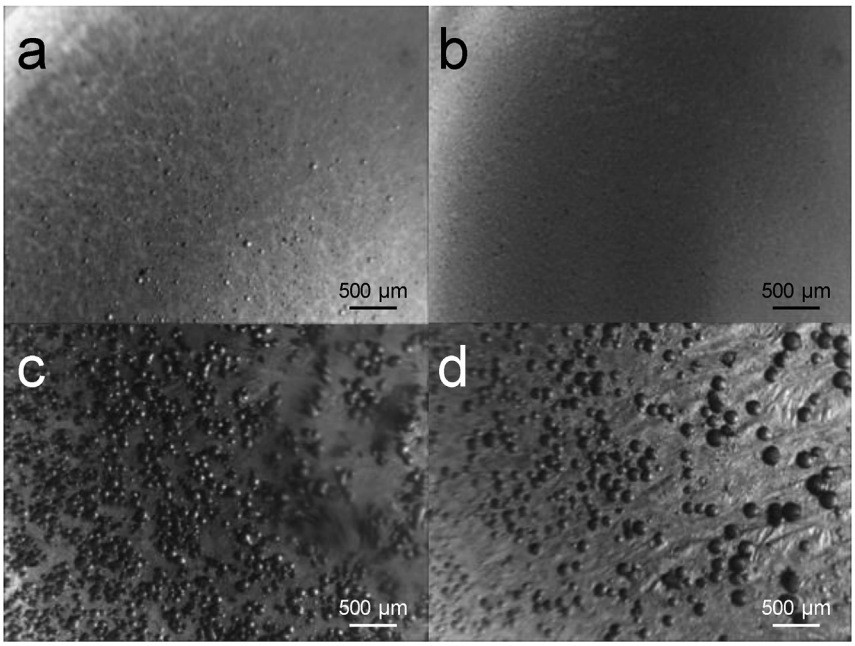

Fig. 3. *In-Situ* optical micrographs of graphene at the water DCE interface, with different combinations of electrolyte in each phase. **a**) Water| DCE, **b**) 0.1 M $LiCl_{(aq)}$| DCE, **c**) Water | 10 mM $BTPPATPBCl_{(DCE)}$, **d**) 0.1 M $LiCl_{(aq)}$ |10 mM $BTPPATPBCl_{(DCE)}$.

(where the radius, $r \gg$ thickness), thus the particle geometry is approximated to a disc.

$$cos\theta = \frac{\gamma_{p|o} - \gamma_{p|w}}{\gamma_{w|o}} \quad (1)$$

$$\Delta E = \pi r^2 \gamma_{w|o}(1 - |cos\theta|) \quad (2)$$

θ and $\gamma_{w|o}$ were measured in the four different water |DCE cells, using sessile and pendant droplet methodologies, respectively. The mean particle diameter was assumed to be 500 nm, from the SEM data. Measurements of θ were performed on freshly cleaved highly oriented pyrolitic graphite (HOPG) as a bulk graphitic material, as a proxy to represent the dispersed graphene flakes. From these measurements (Supporting Information, Figs. S7–S10), ΔE was calculated for graphene flakes at the water DCE interface, using Equation (2), in the presence and absence of electrolyte in both phases. Calculated values of ΔE are plotted in Fig. 4. The changes in ΔE upon addition of electrolyte reflect the changes in θ, as $\gamma_{w|o}$ varied little with and without electrolyte. No increase in ΔE is seen in the presence of organic electrolyte, indicating that the observed changes in particle adsorption have a more complex origin than the simple "surface energy" model discussed above.

To assess the effect of organic electrolyte on interactions between graphene flakes at the water|DCE interface, electrostatics must be considered. A recent study in our laboratory has shown that dispersions of pristine graphene in DCE are stabilised by inter-flake electrostatic repulsions [24]. Addition of a sufficient concentration ($\geq 1 \times 10^{-4}$ M) of electrolyte to these organic phase dispersions induced complete aggregation and sedimentation, attributed to a classical screening mechanism of the electrical double layer (EDL) around the particles. We therefore surmise that in the absence of electrolyte, these electrostatic repulsions will oppose the assembly of graphene flakes attached at the liquid|liquid interface, leading to the individual clusters of flakes seen at the interfaces of cells a and b (Fig. 2). Screening of the electrostatic interactions by organic electrolyte negates this repulsive force and allows the interfacial graphene flakes to come into closer contact, thus leading to the largely continuous interfacial films seen in cells c and d (Fig. 2). Additionally, flake aggregation will result in an overall increase in graphene particle size and a greater driving force for attachment of flakes at the liquid|liquid interface, as expressed by Equation (2).

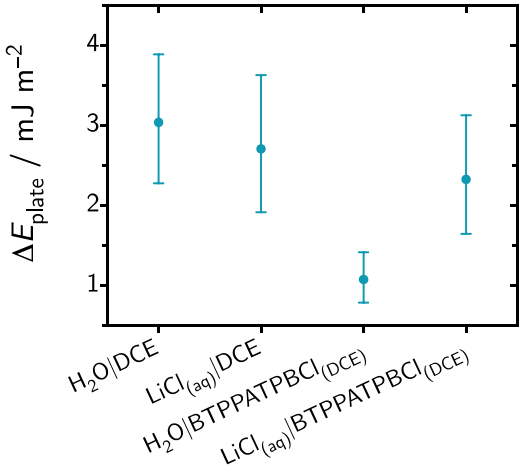

Fig. 4. The stabilisation energy (ΔE) for graphene flakes at the water|DCE interface, in the presence and absence of 0.1 M $LiCl_{(aq)}$ and 10 mM $BTPPATPBCl_{(DCE)}$ electrolytes. The values were calculated using Equation (2), and the θ and $\gamma_{w|o}$ values presented in the Supporting Information, Figs. S8 and S10, respectively.

4. SWCNT assembly

The study into the effect of electrolyte on liquid|liquid interfacial assembly was repeated using a second carbon nano-material, SWCNTs. Dispersions of SWCNTs in DCE were prepared in the same manner as the exfoliated graphene dispersions, with a

starting concentration of 9 μg ml^{-1}. Using the extinction coefficient of 4100 ml mg^{-1} l^{-1} at 660 nm [27], the final dispersion concentration, after centrifugation, was determined to be 6 μg ml^{-1}. The average diameter and length of the dispersed nanotubes were 6 (±3) nm and 700 (±300) nm, respectively, as determined by AFM measurements. An example AFM micrograph, along with histograms of nanotube diameter and length are shown in Fig. S11.

Following the same procedure described for graphene, SWCNTs were assembled at the four different water|DCE interfaces with varying electrolyte composition. Fig. 5a shows the interfacial SWCNTs 12 h after application of the sonication step used to bring the nanotubes to the water|DCE interface. The interfacial behaviour of the SWCNTs, with respect to the presence of electrolyte in either liquid phase, was markedly different from that of graphene. As can be seen from Fig. 5a–d, complete attachment of the SWCNTs occurred at all four of the water|DCE interfaces, with the presence of electrolyte in either or both liquid phases having no influence on the interfacial attachment behaviour. It should be noted that although the CNT materials appear to adsorb preferentially at the ITIES, there is evidence of some emulsification of the organic phase in the case of Fig. 5b. Additionally, no change in this behaviour was observed upon increasing the concentration of the initial SWCNT dispersion up to 25 μg ml^{-1}.

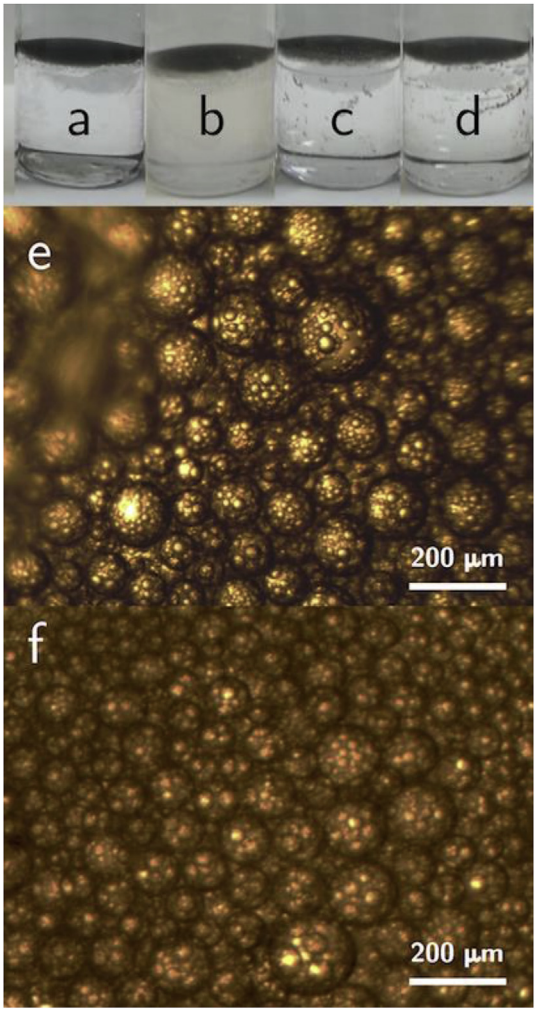

Fig. 5. A-d) Photograph showing attachment of a 3 μg ml^{-1} SWCNT dispersions at the water|DCE interface. Different combinations of electrolyte were present in each cell. **a**) Water|DCE, **b**) 0.1 M $LiCl_{(aq)}$|DCE, **c**) Water|10 mM $BTPPATPBCl_{(DCE)}$, **d**) 0.1 M $LiCl_{(aq)}$|10 mM $BTPPATPBCl_{(DCE)}$. *In-situ* optical micrographs of SWCNTs at the water|DCE (**e**) and 0.1 M $LiCl_{(aq)}$|10 mM $BTPPATPBCl_{(DCE)}$ (**f**) interfaces.

In-situ optical microscopy of SWCNTs at the water|DCE interfaces also revealed very similar interfacial morphologies in the absence and presence of electrolyte (Fig. 5e and f). In each case, the bulk liquid|liquid interface was transformed into multiple emulsified droplets, with smaller droplets embedded in bigger ones, forming "raspberry-like" structures. These droplets are reminiscent of those formed in the presence of graphene, though the density of droplets is far greater in the presence of SWCNTs. We attribute this to a greater stabilisation of the droplets by interfacial SWCNTs, compared to graphene. Since the SWCNTs were originally dispersed in the DCE phase and θ of the water |SWCNT |DCE interface was 139° (Supporting Information, Fig. S13, Table S1), showing that the nanotubes are wetted more by the DCE phase, the multiple emulsions observed are assigned as oil|water|oil type [34].

The stabilisation energy of the interfacial SWCNTs was estimated, at the four different water|DCE interfaces, using Equation (3), where L and R are the length and radius, respectively, of the SWCNTs [32]. This equation is a variant of Equation (2), applicable for the rod-like geometry of the SWCNTs, and assumes that the SWCNTs bind to the liquid|liquid interface with their long axis parallel to the interfacial plane, because of their high aspect ratio [32,35].

$$\Delta E = 2\pi RL\gamma_{w|o}\left(\frac{\pi\theta}{180^{\circ}}\cos\theta - \sin\theta\right) \quad (3)$$

θ was measured on a SWCNT film, which was prepared at the water|DCE interface and transferred onto a Si/SiO_2 substrate, with the measured values presented in the Supporting Information (Fig. S14 and Table S1). Using these values, the $\gamma_{w|o}$ values presented previously (Fig. S9) and the average diameter and length of the SWCNTs (Fig. S11), ΔE was calculated for SWCNTs at the four different water|DCE interfaces. These values are presented in Table 1. It is clear that ΔE is similar at each water|DCE interface (at least 10^6 kT), with the presence of electrolyte in either liquid phase not significantly affecting the stabilisation energy. This trend (or lack of one) is reminiscent of that seen for graphene [36].

The adsorption energies calculated for both types of nanocarbon, on a per flake or per tube basis are quite similar, but when normalized per unit area (see Table 1 and Fig. 4) are found to be one to two orders of magnitude greater for the SWCNTs, compared to the graphene flakes. Furthermore, the area normalized values calculated for the SWCNTs, are relatively insensitive to the presence of the electrolyte. This may explain why the nanotubes are found to partition preferentially to the interface in all four experimental configurations (with/without electrolyte in each of the solution phases), while addition of organic electrolyte is required to favour the interfacial adsorption of the graphene samples. This result is surprising, however, since the absolute adsorption energies in both cases (per flake and per tube) are substantially higher than kT (10^{-16} J compared to 10^{-21} J). The standard "surface energy" model of solid adsorption at liquid/liquid interfaces would normally suggest that platelet adsorption is favoured over tube adsorption, due to the greater area of liquid contact displaced in the former case.

Table 1
Desorption energies into the DCE phase of a SWCNT at various liquid|liquid configurations.

Sample	Configuration	E_{ads}/mJ m^{-2}
SWCNTs	DCE|water	133
SWCNTs	DCE|0.1 M LiCl	127
SWCNTs	10 mM BTPPABCl|water	149
SWCNTs	10 mM BTPPABCl |0.1 M LiCl	150

The observations herein suggest that the physics of particle adsorption is not simply dictated by interfacial tension effects. Electrolyte addition only has a modest effect on interfacial tension (approximately 3%, comparable with the standard deviation of our measurement, see Fig. S8), which is consistent with the accepted picture of weak adsorption of the constituent ions at the water/DCE interface. Electrolyte has a stronger effect on the contact angle of the two phases with respect to graphite (see Fig. S10), changing the cosine of the contact angle term by approximately 10%. It is notable that organic electrolyte, when added in the absence of aqueous phase electrolyte, has the strongest effect, increasing the water contact angle by approximately 10°. We are unaware of prior studies of the effect of organic electrolyte on water/organic contact angles, although the effect of aqueous phase electrolytes on this parameter has been documented. Svitova et al. have explored the effect of aqueous electrolyte on the water/silicone oil contact angle, measured on a variety of silicon substrates, finding no strong effect on contact angle when an "indifferent" electrolyte such as KCl was present [37]. By contrast, stronger specific interactions between Ca^{2+} ions and the substrates meant that the addition of $CaCl_2$ generally (although not exclusively) increased the surface hydrophilicity. Similarly, Borisenko et al. studied the water/diiodomethane contact angle as a function of electrolyte concentration on a variety of doped diamond-like carbon surfaces: a small increase in hydrophilicity was observed on addition of NaCl, this effect was larger (although $\leq 5°$) when $CaCl_2$ was used [38]. Our observation of a more significant (10°) change with organic electrolyte indicates a strong adsorption of this electrolyte on carbon surfaces, which is consistent with previous reports from our laboratory on the effect of SWCNTs on ion transfer at the water/organic interface, and can be assigned to π-π interactions between the nanotube and the aromatic ions [39].

While the presence of electrolyte in the organic phase might affect the microscopic structure of particles at the water|oil interface, the apparent insensitivity of the adsorption of SWCNTs to the presence of the electrolyte, as opposed to graphene, may be attributed to weak electrostatic repulsion between the individual nanotubes/small bundles in the interfacial layer and to the strong inter-tube van der Waals attraction [40], which has been suggested to induce nanotube aggregation into bundles at the liquid/liquid interface [41]. We suggest this difference in adsorption mode, and consequential sensitivity to electrolyte, reflects the different structures of the materials. To displace the maximal liquid contact area, the graphene platelets may be assumed to adsorb parallel to the interface. The terminations of graphene sheets often contain oxygen functionalities, because of the "unsatisfied valence" at the lattice edge, which acquire charge in solution. This effect explains the sensitivity of the interfacial adsorption to electrolyte: it is assumed that the excess charge is negative, thus it is interesting that the organic cation has a marked effect on interfacial graphene adsorption, whereas the adsorption is insensitive to the presence of the aqueous electrolyte. On the other hand, the flexible CNT structures are able to "bundle" without reducing the displaced liquid contact area. Moreover, even though charges due to oxygen or other heteroatoms are most likely to be concentrated at the open ends of the CNTs, these ends only constitute a small fraction of the overall perimeter of the CNTs – unlike the graphene case - which may explain the insensitivity of CNT adsorption to the presence of

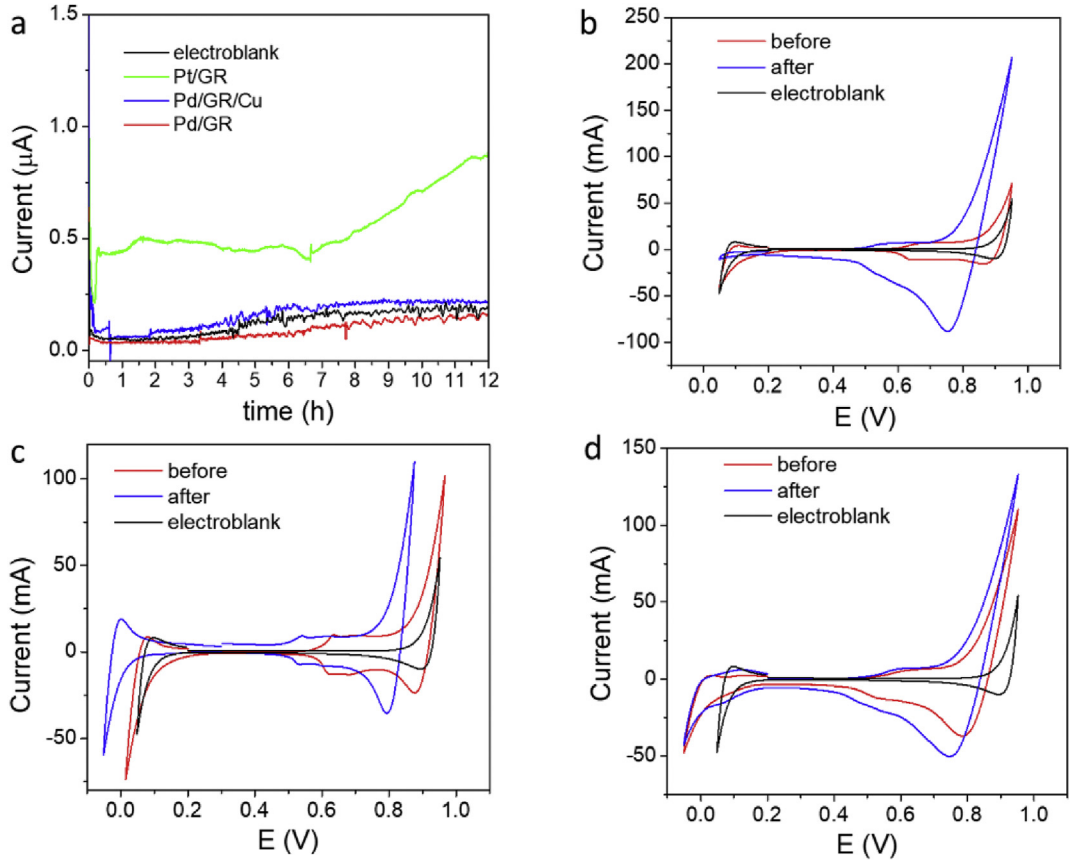

Fig. 6. Chronoamperometric (a) and voltammetric (b–d) responses of the ITIES assembled GR-based catalyst materials during (a) 12 h of oxidation (+0.7 V and +0.8 V) and CVs (b–d) before and after with the following materials adsorbed at the interface to function as bipolar electrodes: (b) Pd-modified graphene, (c) Pt-modified graphene, (d) Pd– and Cu-modified graphene. In each case "blank" corresponds to the response in the absence of the adsorbed graphene materials.

electrolyte.

4.1. Interfacial catalysis with carbon nanomaterials

The catalytic and electrocatalytic properties of doped nanocarbons are of interest. Adsorption of such materials in an ITIES cell allows them to function as bipolar electrodes: in this context, we have investigated the oxidation of the organic phase by application of a positive Galvani potential (+0.7 to +0.8 V, defined as is conventional in ITIES electrochemistry as the potential of the aqueous phase with respect to the organic) for 12 h. Fig. 6a shows the chronoamperometric response from these long-term organic phase oxidation experiments. For these experiments, the modified CVD graphene samples (see Experimental section) were used, to give a well-defined sample, which can be oriented "up" or "down" with respect to the interface. The compositions of cells and interface-assembled composites' names are given in Table 2.

The voltammetric response of the interface before and after the application of this potential difference is shown in Fig. 6b–d for the various modified graphenes used as bipolar electrodes. Evaluating a CV acquired from the ITIES, the potential window is limited by the transfer of supporting electrolyte ions (bis(triphenylphosporanylidene)ammonium cation and tetrakis (4- chlorophenyl)borate anion).

Hexane was added (10 wt%) to the organic phase but no change in the NMR signal due to hexane, or formation of partially oxidised products such as hexanol, was observed. By contrast, the DCB solvent was found to be susceptible to oxidation in the presence of the metal-decorated graphene samples. The presence of the solids without application of a potential did not cause any detectable oxidation, indicating that the metal-modified graphenes function as bipolar electrodes, which catalytically oxidise the DCB. Integrating the currents of chronoamperometric curves (Fig. 6a), the total charges passed are calculated, yielding 5.38, 23.6, 3.74, and 6.88 mC for CVD graphene, Pt/GR, Pd/GR, and Pd/GR/Cu assembled interfaces, respectively. Comparison of the positive vertex of the CVs' after 12 h of electrolysis (Fig. 6b–d) shows that larger currents are observed, suggestive of products derived from DCB oxidation. Fig. 7 shows the detail of the NMR spectra of the organic and aqueous phases: signals associated with products can be discerned, most notably in the case of the Pd/G/Cu sample. The new features at a chemical shift of 2.1–2.2 are consistent with the formation of acetic acid [42], seen in both the aqueous and organic phases, which is reasonable given the partition coefficient of this molecule [43]. A new spectral feature at a chemical shift 8.0 to 8.2 is assigned to formic acid. Application of a 12 h potential to an "electroblank" cell, i.e. with no adsorbed materials at the interface, gave only a weak spectroscopic response, assigned to formic acid [42]. The results suggest that the partial oxidation of DCB by metal-decorated graphene composites produces some partial oxidation products, which we interpret as formic and acetic acid, and that the application of the potential to a catalyst-free interface produces only formic acid, thus changing the selectivity of this partial oxidation process. We note that CuO has been reported as a catalyst for the thermally driven partial oxidation of chlorinated aromatics, including DCB, at temperatures as low as 200 °C [44]. Partial oxidation to acetate and formate has been described using Ti-doped iron oxides at similar temperatures [45]. Total oxidation of chlorinated aromatics, including, DCB, has been reported at higher temperatures (350 °C–500 °C) over silica-supported copper [46]. Other transition metal oxide based catalysts have been reported for the thermal oxidation process [47–49]. Although there is ample literature on the reductive voltammetry of chlorinated aromatic compounds, with reduction typically preceding via a dechlorination process [50], the oxidative electrochemistry of these compounds is less well documented. We note, however, that one very recent report describes ambient temperature electro-oxidation of DCB, under controlled current conditions, with Fenton-type reactions of hydroxyl radicals implicated in the oxidation process [51]. Further work is required to understand the process operating in the presence of the metals under the bi-phasic conditions used here, but the preliminary evidence suggests that a slow oxidation occurs.

Table 2
The cell compositions for the ITIES catalysis experiments combined with NMR measurements. The double vertical bar denotes the polarisable liquid-liquid interface.

Sample name (name of the catalyst)	Configuration
blank (without oxidation)	10 mM BTPPATPBCl (90%DCB+9%hexane+1% hexanol) ‖6 M LiCl (99% water+1% hexanol)
electroblank (with oxidation)	10 mM BTPPATPBCl (90%DCB+10%hexane) ‖ 6 M LiCl
Pt/GR	10 mM BTPPATPBCl (90%DCB+10%hexane) ‖ 6 M LiCl
Pd/GR	10 mM BTPPATPBCl (90%DCB+10%hexane) ‖ 6 M LiCl
Pd/GR/Cu	10 mM BTPPATPBCl (90%DCB+10%hexane) ‖ 6 M LiCl

5. Conclusions

The assembly of carbon nanomaterials at the ITIES is described: SWCNTs are seen to adsorb strongly at the liquid-liquid interface, whereas the adsorption of graphene flakes is very sensitive to the presence of electrolyte within the organic phase. Organic phase electrolyte has been shown to induce sedimentation of dispersions of graphene, a phenomenon interpreted in terms of a classical "double-layer" explanation of particle stability due to residual charges existing at the edges of the graphene flakes. In the case of a

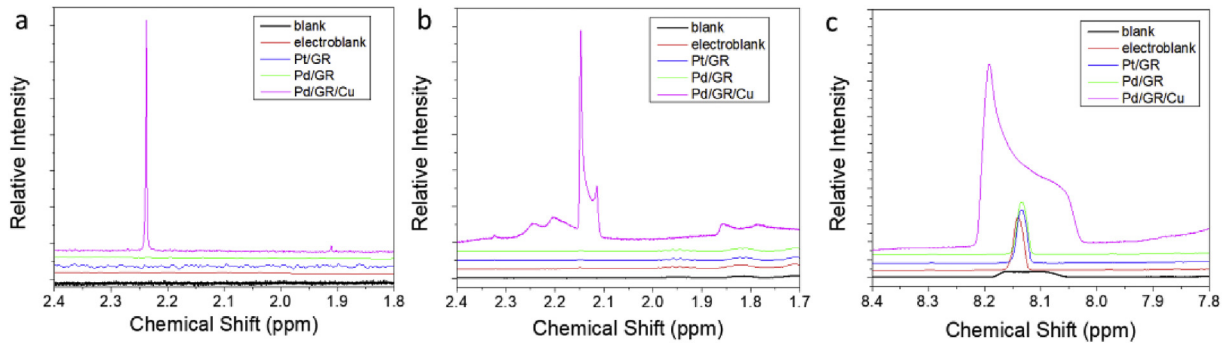

Fig. 7. NMR spectra of samples measured after 12 h oxidation, except for the case of the blank specimen. The samples were collected from aqueous (a) and organic (b, c) phases.

dispersion in contact with an aqueous phase, the bi-phasic case promotes interfacial adsorption, rather than sedimentation, of the graphene. These assembled materials can function efficiently as bipolar electrodes, using modest applied potential differences, because the potential is dropped within the vicinity of the materials in the ITIES case. Metal-decorated CVD graphene samples are shown to induce the partial oxidation of the chlorinated organic solvent: this approach could present an interesting, low energy route for the oxidation of toxic organic materials, further studies are underway to assess the feasibility of this interfacial route to oxidation.

Acknowledgements

We thank the EPSRC for support (grant references EP/K007033/1 and EP/N032888/1) and the Educational Trust Fund (Nigeria) for a PhD scholarship for A.K.R.

Appendix A. Supplementary data

Supplementary data related to this article can be found at https://doi.org/10.1016/j.electacta.2019.04.035.

References

[1] M. Fleischmann, J. Ghoroghchian, D. Rolison, S. Pons, Electrochemical behaviour of dispersions of spherical microelectrodes, J. Phys. Chem. 90 (1986) 6392–6400.
[2] S.E. Fosdick, K.N. Knust, K. Scida, R.M. Crooks, Bipolar electrochemistry, Angew. Chem. Int. Ed. 52 (2013) 10438–10456.
[3] G. Loget, J. Roche, E. Gianessi, L. Bouffier, A. Kuhn, Indirect bipolar electrodeposition, J. A m. Chem. Soc. 134 (2022) 20033–20036
[4] Z. Samec, Electrochemistry at the interface between two immiscible electrolyte solutions, Pure Appl. Chem. 76 (2004) 2147–2180.
[5] F. Reymond, D. Fermín, H.J. Lee, H.H. Girault, Electrochemistry at liquid-liquid interfaces: methodology and potential applications, Electrochim. Acta 45 (2000) 2647–2662.
[6] Z. Samec, Electrical double layer at the interface between two immiscible electrolyte solutions, Chem. Rev. 88 (1988) 617–632.
[7] G.M. Luo, S. Malkova, J. Yoon, D.G. Schultz, B.H. Lin, M. Meron, I. Benjamin, P. Vanysek, M.L. Schlossman, Ion distributions near a liquid-liquid interface, Science 311 (2006) 216–218.
[8] M. Faraday, Experimental relations of gold (and other metals) to light, Phil. Trans. Roy. Soc. Lond. 147 (1857) 145–181.
[9] S.U. Pickering, Emulsions, J. Chem. Soc. Trans. 91 (1907) 2001–2021.
[10] B. Su, J.P. Abid, D.J. Fermín, H.H. Girault, H. Hoffmannová, P. Krtil, Z. Samec, Reversible voltage-induced assembly of Au nanoparticles at liquid vertical bar liquid interfaces, J. Am. Chem. Soc. 126 (2004) 915–919.
[11] R.A.W. Dryfe, A. Uehara, S.G. Booth, Metal deposition at the liquid-liquid interface, Chem. Rec. 14 (2014) 1013–1023.
[12] J.J. Nieminen, I. Hatay, P.Y. Ge, M.A. Mendez, L. Murtomaki, H.H. Girault, Hydrogen evolution catalyzed by electrodeposited nanoparticles at the liquid/liquid interface, Chem. Commun. 47 (2011) 5548–5550.
[13] Y. Gründer, M.D. Fabian, S.G. Booth, D. Plana, D.J. Fermín, P.I. Hill, R.A.W. Dryfe, Solids at the liquid-liquid interface: electrocatalysis with pre-formed nanoparticles, Electrochim. Acta 110 (2013) 809–815.
[14] X.J. Bian, M.D. Scanlon, S.N. Wang, L. Liao, Y. Tang, B.H. Liu, H.H. Girault, Floating conductive catalytic nano-rafts at soft interfaces for hydrogen evolution, Chem. Sci. 4 (2013) 432–3441.
[15] A.N.J. Rodgers, R.A.W. Dryfe, Oxygen reduction at the liquid-liquid interface: bipolar electrochemistry through adsorbed graphene layers, ChemElectroChem 3 (2016) 472–479.
[16] P. Peljo, M.D. Scanlon, A.J. Olaya, L. Rivier, E. Srnirnov, H.H. Girault, Redox electrocatalysis of floating nanoparticles: determining electrocatalytic properties without the influence of solid supports, J. Phys. Chem. Lett. 8 (2017) 3564–3575.
[17] L.T. Qu, Y. Liu, J.B. Baek, L.M. Dai, Nitrogen-doped graphene as efficient metal-free electrocatalyst for oxygen reduction in fuel cells, ACS Nano 4 (2010) 1321–1326.
[18] R.V. Salvatierra, M.M. Oliveira, A.J.G. Zarbin, One-pot Synthesis and processing of transparent, conducting, and freestanding carbon nanotubes/polyaniline composite films, Chem. Mater. 22 (2010) 5222–5234.
[19] S. Biswas, L.T. Drzal, A novel approach to create a highly ordered monolayer film of graphene nanosheets at the liquid-liquid interface, Nano Lett. 9 (2009) 167–172.
[20] P.S. Toth, Q.M. Ramasse, M. Velický, R.A.W. Dryfe, Functionalization of graphene at the organic/water interface, Chem. Sci. 6 (2015) 1316–1323.
[21] P.S. Toth, M. Velický, Q.M. Ramasse, D.M. Kepaptsoglou, R.A.W. Dryfe, Symmetric and asymmetric decoration of graphene: bimetal-graphene sandwiches, Adv. Funct. Mater. 25 (2015) 2899–2909.
[22] P.S. Toth, M. Velický, M.A. Bissett, T.J.A. Slater, N. Savjani, A.K. Rabiu, A.M. Rakowski, J.R. Brent, S.J. Haigh, P. O'Brien, R.A.W. Dryfe, Asymmetric MoS_2/graphene/metal sandwiches: preparation, characterization, and application, Adv. Mater. 28 (2016) 8256–8264.
[23] P.S. Toth, A.K. Rabiu, R.A.W. Dryfe, Controlled preparation of carbon nanotube-conducting polymer composites at the polarisable organic/water interface, Electrochem. Commun. 60 (2015) 153–157.
[24] A.N.J. Rodgers, M. Velický, R.A.W. Dryfe, Electrostatic stabilization of graphene in organic dispersions, Langmuir 31 (2015) 13068–13076.
[25] F. Reymond, V. Chopineaux-Courtois, G. Steyaert, G. Bouchard, P.A. Carrupt, B. Testa, H.H. Girault, Ionic partition diagrams of ionisable drugs: pH-lipophilicity profiles, transfer mechanisms and charge effects on solvation, J. Electroanal. Chem. 462 (1999) 235–250.
[26] M. Lotya, Y. Hernandez, P.J. King, R.J. Smith, V. Nicolosi, L.S. Karlsson, F.M. Blighe, S. De, Z. Wang, I.T. McGovern, G.S. Duesberg, J.N. Coleman, Liquid phase production of graphene by exfoliation of graphite in surfactant/water solutions, J. Am. Chem. Soc. 131 (2009) 3611–3620.
[27] P.S. Toth, A.N.J. Rodgers, A.K. Rabiu, R.A.W. Dryfe, Electrochemical activity and metal deposition using few-layer graphene and carbon nanotubes assembled at the liquid-liquid interface, Electrochem. Commun. 50 (2015) 6–10.
[28] P.S. Toth, S.J. Haigh, A.K. Rabiu, A.N.J. Rodgers, A.M. Rakowski, R.A.W. Dryfe, Preparation of low-dimensional carbon material-based metal nanocomposites using a polarizable organic/water interface, J. Mater. Res. 30 (2015) 2679–2687.
[29] S.J. Woltornist, A.J. Oyer, J.Y. Carrillo, A.V. Dobrynin, D.H. Adamson, Conductive thin films of pristine graphene by solvent interface trapping, ACS Nano 7 (2013) 7062–7066.
[30] S. Biswas, L.T. Drzal, Multilayered nano-architecture of variable sized graphene nanosheets for enhanced supercapacitor electrode performance, ACS Appl. Mater. Interfaces 2 (2010) 2293–3000.
[31] S.G. Booth, R.A.W. Dryfe, Assembly of nanoscale objects at the liquid/liquid interface, J. Phys. Chem. C 119 (2015) 23295–23309.
[32] B. P Binks, T.S. Horozov (Eds.), Colloidal Particles at Liquid Interfaces, Cambridge University Press, Cambridge, 2006.
[33] M.A. Creighton, Y. Ohata, J. Miyawaki, A. Bose, R.H. Hurt, Two-Dimensional materials as emulsion stabilizers: interfacial thermodynamics and molecular barrier properties, Langmuir 30 (2014) 3687–3696.
[34] B.P. Binks, A.K.F. Dyab, P.D.I. Fletcher, Contact angles in relation to emulsions stabilised solely by silica nanoparticles including systems containing room temperature ionic liquids, Phys. Chem. Chem. Phys. 9 (2007) 6391–6397.
[35] R.K. Wang, H. O Park, W.C. Chen, C. Silvera-Batista, R.D. Reeves, J.E. Butler, K.J. Ziegler, Improving the effectiveness of interfacial trapping in removing single-walled carbon nanotube bundles, J. Am. Chem. Soc. 130 (2008) 14721–14728.
[36] F. Reincke, W.K. Kegel, H. Zhang, M. Nolte, D. Wang, D. Vanmaekelbergh, H. Möhwald, Understanding the self-assembly of charged nanoparticles at the water/oil interface, Phys. Chem. Chem. Phys. 8 (2006) 3828–3835.
[37] T. Svitova, O. Theodoly, S. Christiano, R.M. Hill, C.J. Radke, Wetting behavior of silicone oils on solid substrates immersed in aqueous electrolyte solutions, Langmuir 18 (2002) 6821–6829.
[38] K.B. Borisenko, E.A. Evangelou, Q. Zhao, E.W. Abel, Contact angles of diiodomethane on silicon-doped diamond-like carbon coatings in electrolyte solutions, J. Colloid Interface Sci. 326 (2008) 329–332.
[39] A.K. Rabiu, P.S. Toth, A.N.J. Rodgers, R.A.W. Dryfe, Electrochemical investigation of adsorption of single-wall carbon nanotubes at a liquid/liquid interface, Chemistry Open 6 (2017) 57–63.
[40] T.S. Horozov, R. Aveyard, B.P. Binks, J.H. Clint, Structure and stability of silica particle monolayers at horizontal and vertical octane-water interfaces, Langmuir 21 (2005) 7405–7412.
[41] W. Wang, E.D. Laird, Y. Gogotsi, C.Y. Li, Bending single-walled carbon nanotubes into nanorings using a pickering emulsion-based process, Carbon 50 (2012) 1769–1775.
[42] C.E. Housecroft, E.C. Constable, Chemistry, fourth ed., Prentice Hall, Harlow, 2010.
[43] J.M. Nitsche, G.B. Kasting, A correlation for 1,9-decadiene/water partition coefficients, J. Pharm. Sci. 102 (2013) 136–144.
[44] S.L. Alderman, G.R. Farquar, E.D. Poliakoff, B. Dellinger, An infrared and X-ray spectroscopic study of the reactions of 2-chlorophenol, 1,2-dichlorobenzene, and chlorobenzene with model CuO/silica fly ash surfaces, Environ. Sci. Technol. 39 (2005) 7396–7401.
[45] X. Ma, X. Suo, H. Cao, J. Guo, L. Lv, H. Sun, M. Zheng, Deep oxidation of 1,2-dichlorobenzene over Ti-doped iron oxide, Phys. Chem. Chem. Phys. 16 (2014) 12731–12740.
[46] R.M. Lago, M.L.H. Green, S.C. Tsang, M. Odlyha, Catalytic decomposition of chlorinated organics in air by copper chloride based catalysts, Appl. Catal., B 8 (1996) 107–121.
[47] Y. Loa, N. Zhu, X. Jiang, J. Zhao, Q. Dai, X. Wang, Effect of Ru on the activity of Co_3O_4 catalysts for chlorinated aromatics oxidation, Catal. Sci. Tech. 8 (2018) 4797–4811.
[48] X. Ma, X. Feng, J. Guo, H. Cao, X. Suo, H. Sun, M. Zheng, Catalytic oxidation of 1,2-dichlorobenzene over Ca-doped FeOx hollow microspheres, Appl. Catal., B 147 (2014) 666–676.

[49] H. Zhao, W. Han, F. Dong, Z. Tang, Highly-efficient Catalytic Combustion performance of 1,2-dichlorobenzene over Mesoporous TiO_2–SiO_2 supported CeMn oxides: the Effect of acid sites and redox sites, J. Ind. Eng. Chem. 64 (2018) 194–205.
[50] S.O. Farwell, F.A. Beland, R.D. Geer, Reduction pathway of organohalogen compounds: Part 1, chlorinated benzenes, J. Electroanal. Chem. 61 (1975) 303–313.
[51] H. Zazou, N. Oturan, M.S. Çelebi, M. Hamdani, M.A. Oturan, Cold incineration of 1,2-dichlorobenzene in aqueous solution by electrochemical advanced oxidation using DSA/Carbon felt, Pt/Carbon felt and BDD/Carbon felt cells, Sep. Purif. Tech. 208 (2019) 184–193.